CFD Modeling of Friction Stir Welding of AA1100 Aluminum Alloy to A441 AISI Steel Butt Joint

H. Aghajani Derazkola[a],*, M. Elyasi[b], M. Hosseinzadeh[c]

[a] *Young Researchers and Elite Club, Sari Branch, Islamic Azad University, Sari, Iran.*
[b] *Department of mechanical Engineering, Noshiravani University of Technology, Babol, Iran.*
[c] *Department of Engineering, slamic Azad University of Ayatollah Amoli branch, Iran.*

ARTICLE INFO

ABSTRACT

In the present paper, the effects of friction stir welding (FSW) tool rotational and traverse speeds on heat generation and temperature distribution in welding zone of AA1100 aluminum alloy and A441 AISI joint were studied. Computational fluid dynamics method was used to simulate the process with commercial CFD Fluent 6.4 package. To enhance the accuracy of simulation in this study, the welding line in the work-pieces interface was defined with pseudo melt behavior around the FSW pin tool. Simulation results showed that with increase of the FSW tool rotational speed, more heat was generated heat and the dimensions of the stir zone were enlarged. The calculation results showed that maximum temperature occurred on the advancing side. Moreover, with increasing tool linear speeds the heat generation experienced a downward growth trend. With increasing the traveling speeds the time to reach maximum temperature in the stir zone increased, but the tool rotational speed had no effect on the time to reach maximum temperature. The model outcomes showed that more than 85% of total heat was produced by tool shoulder and that the maximum heat with the selected parameters was 935 kelvin degrees. The computed results showed that the maximum value of strain rate achieved was 29 S-1 for the A441 AISI and 42 S-1 at the AA1100 side.

1. INTRODUCTION

Friction stir welding is a comparatively new solid-state joining process which is extensively used in different industries to join different metal alloys that are hard to weld by conventional fusion welding [1]. It is a highly complex process including several physical phenomena [2]. The complex geometry of some kinds of joints and their three dimensional nature make it difficult to develop an overall system of governing equations for theoretical analysis of the behavior of the friction stir welded joints [3]. The experiments are often time consuming and expensive.

Corresponding author:
E-mail address: h.aghajany@gmail.com (Hamed Aghajani Derazkola).

In order to better understand these factors and the development of models, many researchers worked to simulate the process by computational fluid dynamic (CFD) technique. The first researchers that used the CFD to simulation of FSW process were Smith [5] and North [6]. They modeled the work-pieces as non-Newtonian fluid in their simulations. Seidel and Reynolds [7] predicted the material flow in friction stir welding by a two-dimensional model.

They observed that at the low rotational and linear speed, the composition of the fluids substantially occurs in a horizontal manner. This effect indicates the need for further analysis of the process in three dimensions. Zhang et al. [8] with development of the 2D material flow concluded that the material behind tool had the largest deformation compared to the other parts around the pin. This angular deformation occurs between 300 to 360 degrees. Nandan et al. [9-10] solved the 3D FSW of carbon steel process based on momentum, energy and mass transfer equations.

They defined non-Newtonian fluid for simulation and predicted the viscosity, strain rate, temperature and stir zone of carbon steel during friction stir welding. Nassar et al. [11] studied the FSW of AZ31B Mg according to the Eulerian model and the heat transfer problems. They concluded that by increasing the rotational speed, the weld zone temperature rises, while the increase of linear speed, the weld zone temperature decreases. Ji et al. [12] studied the effect of the FSW tool pin profile on the material flow.

According to the available data, no research has reported the thermal modeling of aluminum to steel joint. The aim of this article is the investigation of the frictional heat generation, temperature distribution, velocity and strain rate of dissimilar FSW joint between the AA1100 aluminum alloy and A441 AISI steel based on the previously developed models. This research was done based on previous model developments and their relation to chemical diffusion equation with plastic deformation during FSW of aluminum to steel with tungsten tool.

2. Governing equations

The computational domain in this study includes the work-piece and the tool inserted inside the work-piece. The dimensions of the plate and the tool used and the thermo-physical properties of the work-piece and the tool material are given in Table 1. Between warm-up after pin-insertion and pin-extraction from the work-piece, the thermal cycles occurred at locations equidistant from the weld centerline. Therefore, the temperature and velocity fields were solved assuming steady state behavior. The plastic flow in a three dimensional manner is represented by the momentum conservation equation in index notation, with i or j = 1, 2 and 3, representing x, y and z directions, respectively [13]:

$$\rho \frac{\partial u_i u_j}{\partial x_i} = -\frac{\partial P}{\partial x_j} + \frac{\partial}{\partial x_i}\left(\mu \frac{\partial u_i}{\partial x_j} + \mu \frac{\partial u_j}{\partial x_i}\right) - \rho U_1 \frac{\partial u_j}{\partial x_1}$$

[1]

In Eq. (1), u is the velocity, ρ is the density, U_1 is the welding velocity, and P is the pressure and μ refers to non-Newtonian viscosity that can be determined from flow stress and effective strain rate as follows [14]:

$$\mu = \frac{\sigma_e}{3\dot{\varepsilon}}$$

[2]

The calculation of viscosity requires local value of the strain rate and temperature. In Eq. (2), σ_e indicated the flow stress proposed by Sheppard and Wright [15-16]:

$$\sigma_e = \frac{1}{\alpha} arc \sinh\left(\frac{Z}{A}\right)^{\frac{1}{n}}$$

[3]

Where A, a, and n are material constants, and Z is the Zener – Hollomon parameter. The values of the constants for base metals are shown in Table 1.

Table 1. Chemical parameters of the work-pieces

Parameter	AA1100 [17]	A441 AISI [17]
Q (kJ/mol)	158.3	205.2
R (J/K.mol)	8.314	8.314
A (1/S)	5.18e10	0.6e10
n	5.66	1.2
ρ (Kg/m3)	2710	7810

The Zener – Hollomon parameter (Z) in Eq. 3. Represents the temperature compensated effective strain rate and is given by [18]:

$$Z = \dot{\varepsilon} exp^{\left(\frac{Q}{RT}\right)} \qquad [4]$$

Here Q = 158.3 kJ/mol [19] is the temperature-independent activation energy, R is the universal gas constant, is the effective strain rate and is given by [13]:

$$\dot{\varepsilon} = \sqrt{\left(\frac{2}{3}\varepsilon_{ij}\varepsilon_{ij}\right)} \qquad [5]$$

Where ε_{ij} is the strain rate tensor, defined as [13]:

$$\varepsilon_{ij} = \frac{1}{2}\left(\frac{\partial u_i}{\partial x_j} + \frac{\partial u_j}{\partial x_i}\right) \qquad [6]$$

According to the materials physical changes during hot working, achieve the relation with mechanical and thermal properties during FSW in simulation procedure will be necessary. Based on this factor, the AA1100 aluminum alloy C_P and K parameters are defined as [20]:

$$C_p = 929.3 - 0.627T + 1.48\times10^{-3}T^2 - 4.33\times10^{-8}T^3 \qquad [7]$$

$$K = 25.2 + 0.398T + 7.36\times10^{-6}T^2 - 2.52\times10^{-7}T^3 \qquad [8]$$

And for A441 AISI steel [17]:

$$C_p = 462 - 8.1T + 3.2\times10^{-4}T^2 + 2.0\times10^{-7}T^3 \qquad [9]$$

$$K = 3.7 + 0.09T - 1.8\times10^{-4}T^2 + 7.8\times10^{-8}T^3 \qquad [10]$$

And for tungsten tool [17]:

$$C_p = 128.3 - 3.279\times10^{-2}T + 4.31\times10^{-6}T^2 \qquad [11]$$

$$K = 153.5 - 9.56\times10^{-2}T + 5.23\times10^{-5}T^2 \qquad [12]$$

The pressure field was obtained by solving the following continuity equation iteratively with the momentum equations for incompressible single phase flow [9]:

$$\frac{\partial v_i}{\partial x_i} = 0 \qquad [13]$$

That v_i is the velocity of plastic flow. The steady single phase momentum conservation equations with reference to a co-ordinate system attached to the heat source may be represented as [21]:

$$\rho C_p \frac{\partial(u_i T)}{\partial x_1} = -\rho C_p U_1 \frac{\partial T}{\partial x_1} + \frac{\partial}{\partial x_i}\left(k\frac{\partial T}{\partial x_i}\right) + Q_i + Q_b \qquad [14]$$

The heat generated at the interface between vertical and horizontal surfaces of the tool pin and the work-piece may be defined as [21]:

$$Q_i = \left[(1-\delta)\eta\tau + \delta\mu_f P_N\right](\omega r - U_1\sin\theta)\frac{A_r}{V} \qquad [15]$$

Where A_r is any small area on the tool pin-work piece interface, r is the radial distance of the center of the area from the tool axis, V is the control-volume enclosing the area A_r, s is the maximum shear stress at yielding and θ is the angle with the negative x-axis in the counter-clockwise direction, η is the mechanical efficiency (The amount of mechanical energy converted to heat energy), δ denotes the spatially variable fractional slip between the tool and the work-piece interface, f is the spatially variable coefficient of friction, ω is the angular velocity, and P_N is the normal pressure on the surface. An estimate of the viscous dissipation of momentum per unit volume, Q_b, has been calculated as [22-23]:

$$Q_b = \frac{d\dot{\varepsilon}_p}{dV} = \beta\mu\varphi \qquad [16]$$

In which φ is given by [24]:

$$\varphi = 2\sum_{i=1}^{3}\left(\frac{\partial u_i}{\partial x_i}\right)^2 + \left(\frac{\partial u_1}{\partial x_2} + \frac{\partial u_2}{\partial x_1}\right)^2 + \left(\frac{\partial u_1}{\partial x_3} + \frac{\partial u_3}{\partial x_1}\right)^2 + \left(\frac{\partial u_3}{\partial x_2} + \frac{\partial u_2}{\partial x_3}\right)^2 \qquad [17]$$

Table 2. Chemical parameters of the work-

Parameters	Value
Q_1 (KJ/ mol)	280.5
Q_2 (KJ/ mol)	276.3
A_1 (cm2/s)	148.0
A_2 (cm2/s)	60.0
Fe purity (At. %)	48
AL purity (At. %)	52

In E$_q$. (16), β is an arbitrary constant that indicates the extent of mixing on the atomic scale. The value of e may tend to 1for a well-mixed system in molecular scale [25]. The mass conservation equation for each work-piece in low concentration is expressed as follows [17]:

$$\frac{\partial\left(u_j C_i\right)}{\partial x_j} = -V\frac{\partial C_i}{\partial x_1} + \frac{\partial}{\partial x_1}\left(D\frac{\partial C_i}{\partial x_j}\right) \qquad [18]$$

V is the vertical speed of the plastic material and D refers to the temperature-dependent chemical diffusion which is defined as [17]:

$$D = A_1 e^{\left(-\frac{Q_1}{RT}\right)} + A_2 e^{\left(-\frac{Q_2}{RT}\right)} \qquad [19]$$

With regard to the atomic percent of aluminum and steel in the junction, the parameters chosen for this simulation were defined in Table 2 [17]:

The total heat generated at the shoulder/work-piece interface has been partitioned between the work-piece and the tool in the ratio given below [21]:

$$q = \frac{\left(\sqrt{k\rho C_p}\right)_{workpiece}}{\left(\sqrt{k\rho C_p}\right)_{tool} + \left(\sqrt{k\rho C_p}\right)_{workpiece}} \qquad [20]$$

Where the subscripts W and T denote the work-piece and the tool, respectively. The analytical expression is based on the steady-state one dimensional heat transfer from point heat source located at the interface of dissimilar metals. The heat flux into the work-piece is estimated to be 45% of the total heat generated. This relation has been examined experimentally by Lienert et al. [25] and was found to be reliable. A heat flux continuity at the shoulder matrix interface yields [21]:

$$k\left.\frac{\partial T}{\partial Z}\right|_{Top} = \frac{J_w}{J_w + J_T}q_1 \qquad \text{in the range RP} \le r \le \text{RS}$$

$$[21]$$

RP and RS represent the tool pin and shoulder radius, respectively and q1 represents the total rate of heat generation at the shoulder–work-piece interface. It is given by [21]:

$$q_1 = \left[\eta\left(1-\delta\right)\tau + \delta\mu_F P_H\right]\left(\omega r - U_1\sin\theta\right) \qquad [22]$$

At the bottom surface, there is a backing plate and the heat transfer coefficient from the bottom of the work-pieces is not the same as for free convection. The values of the heat transfer at bottom of work-pieces were determined by:

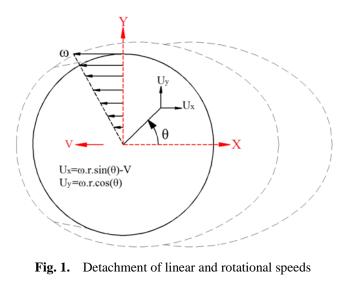$$k\left.\frac{\partial T}{\partial Z}\right|_{Bottom} = h_b\left(T - T_a\right) \qquad [23]$$

Where h_b is the bottom heat transfer coefficient and Ta is the ambient temperature of 298 K. The heat transfer coefficient at the bottom faces depends on the local temperature and is given by the following relation [26]:

$$h_b = h_{b0}\left(T - T_a\right)^{0.25} \qquad [24]$$

Where h_{b0} is the heat transfer parameter for the bottom surfaces. As Eq. (20) shows, this parameter is a constant and it has a different unit compared to the heat transfer coefficient which is spatially variable. At the top surface, heat transfer is due to both convection and radiation and is given by:

$$-k\left.\frac{\partial T}{\partial Z}\right|_{Top} = B\epsilon\left(T^4 - T_a^4\right) + h_t\left(T - T_a\right) \qquad [25]$$

B is the Stefan–Boltzmann constant (5.67*10–16 J.K–4.m–2.s–1), ε is the emissivity and h_t is the convective heat transfer coefficient at the top surface. The computed temperature values were found to be insensitive to the values of h_t and its value was taken as zero for simplicity. During the simulation, linear and rotational speeds of the tool pin and shoulder were performed separately. For this purpose, the sums of the rotational and linear speeds as separate components in a Cartesian coordinate system were defined. Fig. 1 shows the
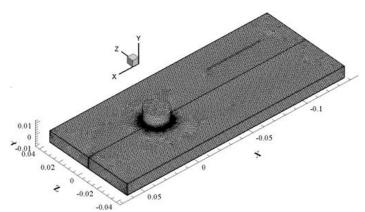
Fig. 1. Detachment of linear and rotational speeds

Fig. 2. The meshed model of the process

detachment of linear and rotational speeds into a unified coordinate system. Velocities at the tool pin periphery have been defined in terms of tool translation velocity and the tool pin angular velocity [27]:

$$u = \left(\omega R_p \sin\theta - U_1 \right) \qquad [26]$$

$$v = \left(\omega R_p \cos\theta \right) \qquad [27]$$

$$w = k \left(\frac{\omega}{2\pi} \right) R_P \qquad [28]$$

K in Eq. (28), represents a pitch the threads on the pin tool. Similarly, at the shoulder–work-piece interface, the velocity boundary conditions may be written as [27]:

$$u = \left(\omega r \sin\theta \right) \qquad [29]$$

$$v = \left(\omega r \cos\theta \right) \qquad [30]$$

At all other surfaces, the temperatures are set to ambient temperature (298 K).

3. Process modeling and mesh generation

According to the FSW pattern, the tool passed three main steps from the start to the end of welding. The first step is called plunging which means the joint line is penetrated by tool. The second step is mixing of the joint line and the last step is tool exit after completion of the welding. In this study, the first and last phases of tool situation have been neglected and the simulation proceeds on the tool situation during moving forward. In this model, a frustum pin with 2o tilt angel was designed as the FSW tool with 10 mm shoulder diameter. The big diameter of pin was 6 mm, the small diameter was 4 mm and the pin height was 2.8 mm. The base metal was assumed as non-Newtonian fluid with visco-plastic behavior and density based on the AA1100 aluminum alloy. The Tetrahedral/Hybrid elements with T-grid combination shape were used for the mesh

Table 3. Tool parameters

Tool Parameters	Value
ω, rpm	500, 630, 710, 800
V, mm/min	25
Work-piece Length for each one (mm)	200
Work-piece width for each one (mm)	100
Work-piece thickness for each one (mm)	3
Tool shoulder radius	10
Pin big radius	3
Pin small radius	2
Pin height	2.8
Tool tilt angle	2
δ_0	2.3
η	0.004
μ_0	0.41
ε	0.5
P_N, N	10e8

Table 4. Physical and mechanical properties of the base metals

Parameter	AA1100 [28-29]	A441 AISI [30]	Tungsten [17]
ρ (Kg/m^3)	2710	7810	19400
Melt point (^{o}C)	657	1400	3685
σ_Y (MPa)	34	344	-
σ_{UTS}	90	580	-
τ (MPa)	62	360	-
Elongation (%)	35	15	-

generation of the tool and the work-piece. The region close to the pin tool and the tool itself required a much finer mesh to evaluate the heat transfer model and viscous flow. A sizing function on the tool and work-piece was used to generate the different volume sizes. The sizing function uses a start size, growth rate and maximum size. For the fine mesh depicted in Fig. 2, the start size was 0.1 mm, the growth rate 1.3 mm, and the maximum size was 1.5 mm. For this meshing scheme, the total number of volumes for the latter case was 3, 864, and 200 volumes. The cross section of the model with meshes and the used parameters are shown in Fig. 3 and Table 3, respectively.

4. Experimental procedure
In this research, AA1100 aluminum alloy and A441 AISI plates with 3mm thickness were cut into dimensions measuring 200 mm long and 100 mm wide. The physical and mechanical properties of the base metals are presented in Table 4.

A flexible clamping system made of high carbon steel was designed to clamp the plates in their proper positions. Single-pass friction stir butt welds were conducted using a milling machine, in control position, and the FSW tool was made of tungsten carbide. The tool has a 20 mm diameter shoulder with a conical cavity and a conical probe measuring 4 to 6 mm in diameter and 2.8 mm in length. In these experiments, the steel plates were located on the advancing side. For conducting the experiments, a single factor experimental design was used. During experimental tests, the tool tilt angle, the tool offset, the welding force
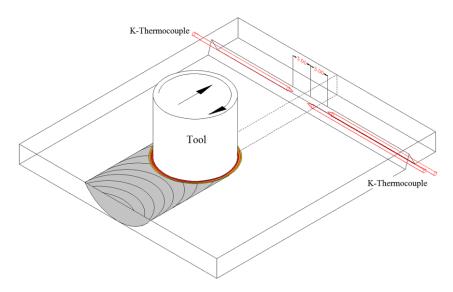
Fig. 3. The thermocouple set up

and the tool traveling speed were 2o, 0 mm and 12e+06 N, respectively.

The K-type thermocouples were used to measure the temperature at mid-plate thickness for both sides of the sheets. A groove was prepared in the middle of the sheets that were supposed to be welded and one thermocouple was determined as origin. For more accurate study of the heat flow, two more thermocouples were used. Each of them was placed within 3 cm distance from the indicator thermocouple at aluminum and steel side. The thermocouple set up is shown in Fig. 3.

5. Results and discussion
5.1. The heat generation rate
For the conditions in this work, the computed heat generation rates of each part of the tool are presented in Fig. 4. The proportion of the heat generated at the tool shoulder and the pin surfaces is determined by the tool geometry and the welding variables. The results show that the tool shoulder generated more heat in the aluminum side than in the steel side. On the other hand, the tool shoulder generated more heat than pin in both sides. This phenomenon is related to the more contact between the tool shoulder and work-pieces. Heat generation portion of each part increases with tool

rotational speed. The reason for this increase with is clear from Qi. In general, it can be concluded that more amount of heat has been generated in the aluminum side.

5.2. Internal temperature Fields
Fig. 5 shows the amount of heat generated in 800 rpm tool rotational speed after 10 and 20 seconds after the start of the welding.

It is clear that amount of the heat generated by the pin tool is much smaller than the tool shoulder. The results revealed that the lowest temperature was produced at the bottom of the pin, near the nethermost of the work-piece. It can be said that maximum heat was generated during this process by the tool shoulder due to more contact area between this region and work-pieces. The results showed that the temperature diffusion starts along with the heat generated from upper area of the joint. After a few seconds, the penetrations of heat into the work-piece are increased and ambient temperature raises and the heat infiltrates to the work-pieces lower areas. The difference between physical and thermal properties of the work-piece caused diffusion; distribution and the amount of frictional heat were not identical. This trend is also seen in the FSW of AA1100 aluminum alloy and A441 AISI steel. As can be
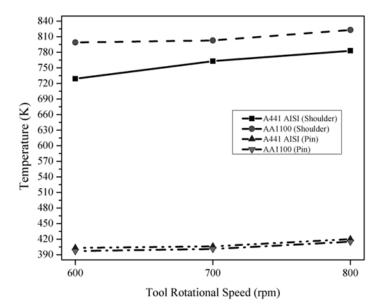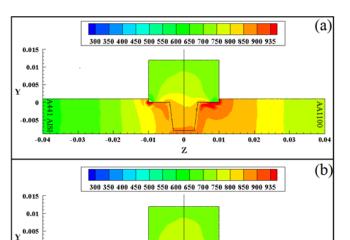
Fig. 4. The heat generation rate

Fig. 5. Cross section view of the internal generated heat at (a) 10s and (b) 20s after the start of the welding

seen in Fig. 5, the diffusion of temperature on the aluminum side is more than the steel side. This is due to the lower flow stress of aluminum compared to steel and greater aluminum heat transfer coefficient compared to steel base metal. With increasing the tool rotational speed, the generated heat increases and due to the changes in the extent of stir zone became bigger.

Fig. 6 shows the comparison of computed peak temperature and real data at the stir zone as function of welding rotational speed and the amount of heat. The results show that the peak temperature increases with an increase in the rotational speed. As can be seen in this figure, the amounts of computed heat generation were in the range of 857 to 942 kelvin for tool rotational speeds between 600 to 800 rpm, respectively. The resulting actual peak
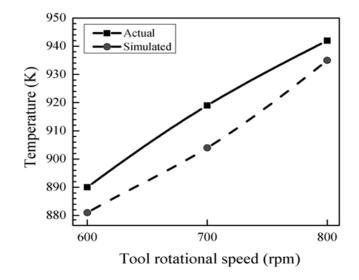
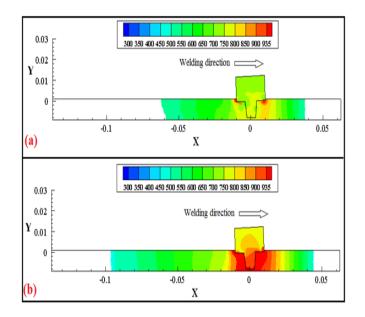**Fig. 6.** Computed and real temperature at different tool rotational speeds

Fig. 7. Temperature distribution in the base metals interface at (a) 10s and (b) 20s after starting welding

temperatures at the stir zone were 881, 904 and 935 K, respectively, for 600, 700 and 800 rpm. In summary, the computed results from a well-tested three-dimensional heat transfer model are in good agreement with real temperature for various welding rotational speeds. The thermal graph of the base metals interface after 10 and 20 seconds from the start of welding joined at 800 rpm is shown in Fig. 7. The results indicated asymmetric hot area at rear and back of the tool axis. The hottest area which indicates plasticized materials is more spread at

the back of the tool compared to the leading of tool. This phenomenon is leading of axial and forging force exerted by the tool to the plastic materials.

5.3. The surface heat flow
The computed temperature profile at the top surface of work-pieces joined at 800 rpm after 10 and 20 seconds is shown in Fig. 8. The temperature profiles on the top surface of the work-piece is compressed in front of the tool and expanded behind it. As mentioned before,
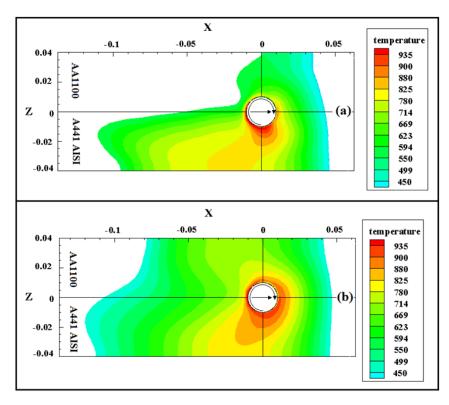
Fig. 8. Temperature distribution at the surface of the base metals (a) 10s and (b) 20s after starting welding

the maximum temperature is produced at the aluminum side and as a consequence of this phenomenon a more expanded heat affected area can be seen at the AA1100 side. This asymmetry results are due to angular variation of heat generation and material flow in dissimilar joints.

5.4. The velocity and strain rate
The computed strain rate history at 800 rpm tool speed is shown at Fig. 9. This trend was observed for both alloys, but the amount of strain rate was different. The maximum value of strain rate achieved was 29 S-1 for A441 AISI side and 42 S-1 at AA1100 side at the top surface of the base metals. It is also observed that strain rates decrease rapidly with depth, which may be attributed to large decrease in velocities away from the shoulder through viscous dissipation. The computed strain rate of the joints which were welded by 600 rpm and 700 rpm were 33 S-1 and 37 S-1 at the steel

side and 21 S-1 and 26 S-1 at the aluminum side, respectively.

In CFD simulation of FSW, pressure is relative and only pressure gradients arise in the computational method. The pressure results have physical significance that featured about the material forging of the plasticized alloy around the tool and the defects formation in joint. Fig. 10 shows the distribution of pressure in the top plane of the work-pieces at 800 rpm tool rotational speed. In general, the amount of pressure is higher in front of the tool compared to the backside of the tool. This phenomenon can be attributed to the forging of the material which causes the plastic material from ahead of tool drawn to the stir zone. The pressure distribution is not asymmetric about the tool axis due to the difference in the physical properties of the base metals. The results show that the maximum pressure was 9e+07 at front of the tool and -1.6e+08 behind the tool.
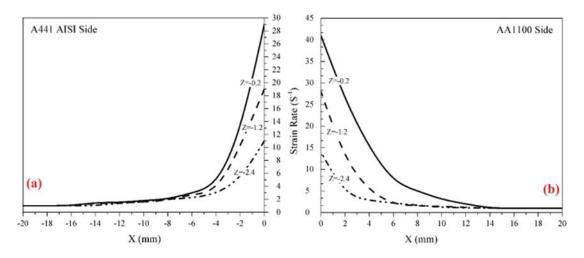
Fig. 9. The strain rate at different faces at (a) A441 AISI and (b) AA1100 base metals
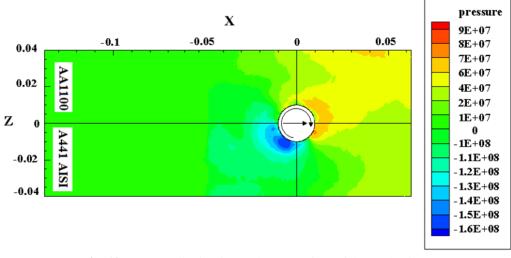

Fig. 10. Pressure distribution at the top surface of the work-pieces

6. Conclusion

In this study, the thermal concept of friction stir welding of aluminum alloy and steel was three dimensionally simulated using computational fluid dynamics. The simulation results are as follows:

1. The study of heat generation tool parts revealed that the heat from the shoulder generated maximum amount of heat, due to the more contact area with the work-piece. The results show that approximately 80 percent of the total heat was generated by the tool shoulder at both aluminum and steel sides.

2. Based on the selected parameters in this study, during FSW of AA1100 aluminum alloy and A441 AISI steel the highest temperature was produced at 800 rpm (942 K), and the lowest temperature was produced at 500 rpm rotational speed (857 K).

3. The heat distribution start from the contact area between the work-piece and the tool shoulder and the temperature diffusion on the aluminum side was more than steel side.

4. The maximum strain rate was obtained at 800 rpm on the top surface of work-pieces. The maximum value of strain rate achieved was 29 S-1 for A441 AISI side and 42 S-1 at the AA1100 side. The maximum pressure was 9e+07 at the front of tool and -1.6e+08 behind the tool.

References

1. S. Golezani, S. M. Arab, Sh. Javadi and F. Kargar, The Effect of Friction Stir Processing

Speed Ratio on the Microstructure and Mechanical Properties of A 430 Ferritic Stainless Steel, Journal of Advanced Materials and Processing, Vol. 2, No. 2, 2014, pp. 39-48.

2. D. Santiago, S. Urquiza, G. Lombera and L. Vedia, 3D Modeling of Material Flow and Temperature in Friction Stir Welding, Soldagem & Inspeção, Vol. 14, No. 3, 2009, pp. 248-256.

3. R. Hamilton, D. MacKenzie and H. Li, Multi-physics simulation of friction stir welding process, Engineering Computations: International Journal for Computer - Aided Engineering and Software, Vol. 27, No. 8, 2010, pp. 967-985.

4. Z. Zhang, H. W. Zhang, A fully coupled thermo-mechanical model of friction stir welding, International Journal of Advanced Manufacturing Technology, Vol. 37, 2008, pp. 279-293.

5. Smith, G. Bendzsak, T. North, J. Hinrichs, J. Noruk and R. Heideman, Heat and Material Flow Modeling of the Friction Stir Welding Process, 11th International Conference on Computer Technology in Welding, Detroit, United State, 1999.

6. T. North, G. Bendzsak and C. Smith, Material Properties Relevant to 3-D Modeling, 2nd International Friction Stir Welding Symposium, Gothenburg, Sweden, 2000.

7. T. U. Seidel, A. P. Reynolds, Two-dimensional friction stir welding process model based on fluid mechanics, Science and Technology of Welding and Joining, Vol. 8, 2003, pp. 175-183.

8. W. Zhang, T. DebRoy, T. A. Palmer and J. W. Elmer, Modeling of ferrite formation in a duplex stainless steel weld considering non-uniform starting microstructure, Acta Materialia, Vol. 53, No. 16, 2005, pp. 4441–4453.

9. R. Nandan, G. Roy and T. DebRoy, Numerical simulation of three dimensional heat transfer and plastic flow during friction stir welding, Metallurgical and Materials Transactions A, Vol. 37, No. 4, 2006, pp. 1247–1259.

10. R. Nandan, G. Roy, T. Lienert and T. DebRoy, Numerical modelling of 3D plastic flow and heat transfer during friction stir welding of stainless steel, Science and Technology of Welding and Joining, Vol. 11, No. 5, 2006, pp. 526-537.

11. H. W. Nassar, M. K. Khraisheh, Simulation of Material Flow and Heat Evolution in Friction Stir Processing Incorporating Melting, Journal of Engineering Materials and Technology, Vol. 134, 2012, pp. 61-67.

12. S. D. Ji, Q. Y. Shi, L. G. Zhang, A. L. Zou, S. S. Gao and L. V. Zan, Numerical simulation of material flow behavior of friction stir welding influenced by rotational tool geometry, Computational Materials Science, Vol. 63, 2012, pp. 218–226.

A. Arora, Z. Zhang, A. Deb and T. DebRoy, Strains and strain rates during friction stir welding, Scripta Materialia, Vol. 61, 2009, pp. 863–866.

13. O. C. Zienkiewicz, I. C. Cormeau, Visco-Plasticity Solution by Finite-Element Process", Archives of Mechanics, Vol. 24, 1972, pp. 872-889.

14. T. Sheppard, D. S. Wright, Determination of Flow-Stress .1. Constitutive Equation for Aluminum Alloys at Elevated-Temperatures, Metals Technology, Vol. 6, 1979, pp. 215-223.

15. T. Sheppard, D. S. Wright, Determination of Flow-Stress .2. Radial and Axial Temperature Distribution during Torsion Testing, Metals Technology, Vol. 6, 1979, pp. 224-229.

16. E. A. Brandes, G. B. Brool, Smithells Metals Reference Book, 8th Ed, Elsevier, Oxford, 2004.

17. Zener, J. H. Hollomon, Effect of Strain Rate upon Plastic Flow of Steel, Journal of Applied Physics, Vol. 15, 1944, pp. 22-32.

18. T. Sheppard, D. S. Wright, Determination of flow stress: Part 1 constitutive equation for aluminum alloys at elevated temperatures, Metals Technology, Vol. 6, 1979, pp. 215-223.

19. Davis, J. R., Nonferrous, Alloys and Special-Purpose Material, ASM Handbook, Vol. 2, Ohio, 1990.

20. R. Nandan, G. Roy, T. J. Lienert and T. Debroy, Three-dimensional heat and material flow during friction stir welding of mild steel, Acta Materialia, Vol. 55, 2007, pp. 883–895.

21. H. S. Carslaw, J. C. Jaeger, Conduction of heat in solids, 2end Ed, Oxford, Clarendon Press, 1959, pp. 87–89.

22. R. Ayer, H. W. Jin, R. R. Mueller, S. Ling and S. Ford, Interface structure in a Fe–Ni friction stir welded joint, Scripta Materialia, Vol. 53, 2005, pp. 1383-1387.

23. R. Nandan, B. Prabu, A. De and T. Debroy, Improving Reliability of Heat Transfer and Materials Flow Calculations during Friction Stir Welding of Dissimilar Aluminum Alloys, Welding Journal, Vol. 86, 2007, pp. 313-322.

24. T. J. Lienert, W. L. Stellwag, B. B. Grimmett and R. W. Warke, Friction Stir Welding Studies on Mild Steel, Welding Journal, Vol. 82, 2003, pp. 1s-9s.

25. R. Schuhmann, Metallurgical Engineering, Vol. 1: Engineering Principles, Cambridge press, Addison-Wesley Press, 1952.

26.
27. B. C. Liechty, B. W. Webb, Modeling the frictional boundary condition in friction stir welding, International Journal of Machine Tools and Manufacture, Vol. 48, 2008, pp. 1474-1485.
28. P. I. Temple, Aluminum and aluminum alloys, 10st ed., AWS Welding Handbook, Ohio, 1998, Chap1.
29. G. E. Totten, S. MacKenzie, Handbook of Aluminum, Vol. 2, Marcel Dekker, New York, 2003, Chap 6.
30. Y. Weng, H. Dong and Y. Gan, Advanced Steels, Springer-Verlag Berlin Heidelberg and Metallurgical Industry Press, 2011, pp.3-35.